JPhys Materials

PAPER • OPEN ACCESS

Tuning the spin texture of graphene with size-specific Cu_n clusters: a first-principles study

To cite this article: Ramasamy Murugesan *et al* 2023 *J. Phys. Mater.* **6** 035005

IOP Publishing J. Phys. Mater. 6 (2023) 035005 https://doi.org/10.1088/2515-7639/acd8f2

Journal of Physics: Materials

OPEN ACCESS

RECEIVED
25 January 2023

REVISED
2 May 2023

ACCEPTED FOR PUBLICATION
25 May 2023

PUBLISHED
8 June 2023

PAPER

Tuning the spin texture of graphene with size-specific Cu_n clusters: a first-principles study

Ramasamy Murugesan[1,*], **Ewald Janssens**[2], **Joris Van de Vondel**[2], **Valeri Afanas'ev**[1,3] and **Michel Houssa**[1,3]

[1] Semiconductor Physics Laboratory, Department of Physics and Astronomy, KU Leuven, Celestijnenlaan 200D, B-3001 Leuven, Belgium
[2] Quantum Solid-State Physics, Department of Physics and Astronomy, KU Leuven, Celestijnenlaan 200D, B-3001 Leuven, Belgium
[3] Imec, Kapeldreef 75, B-3001 Leuven, Belgium
[*] Author to whom any correspondence should be addressed.

E-mail: ramasamy.murugesan@kuleuven.be

Keywords: graphene, copper cluster, induced spin–orbit coupling, spin texture, spin lifetime anisotropy

Supplementary material for this article is available online

Abstract

The size dependent interaction of Cu_n ($n = 1-5$) clusters with pristine and defective (C-vacancy) graphene is studied by employing density functional theory. The computed binding energies are in the range of ∼0.5 eV for pristine graphene and ∼3.5 eV for defective graphene, indicating a much stronger interaction in the later system. The induced spin–orbit coupling interaction, due to the proximity of the Cu_n cluster, is studied with non-collinear spin-polarized simulations. The clusters cause a spin splitting in the order of few meV. The resultant low energy bands spin textures are also computed, and a spin–valley coupling in the case of even atom clusters on pristine graphene is predicted, leading to the emergence of a spin lifetime anisotropy. For defective graphene, a complete out-of-plane spin texture and a large spin splitting of 40–100 meV is obtained for Cu_n ($n = 1, 2, 3, 5$) clusters due to local magnetic moment. On the other hand, for Cu_4/defective graphene, having no net magnetic moment, the spin–valley coupling prevails close to the band edges.

1. Introduction

Ever since the discovery of graphene [1], a large family of 2D materials have been designed and studied, with each demonstrating unique properties for technological applications [2–5]. The 2D nature of these materials renders them highly sensitive to their environment, and allows to tune their properties through close proximity to other materials, e.g. to induce magnetic ordering [6, 7], superconductivity [8–10], and topological states [11–14]. These effects could be combined and engineered for exploring new phenomena [15–17]. In particular, in the field of spintronics, graphene with its Dirac cone and long room temperature spin lifetime makes it a suitable candidate for passive spintronics. However, to realize innovative manipulation and generation of spin currents, its spin–orbit coupling (SOC) needs to be amplified by orders of magnitude. Several research efforts have been made to induce SOC by proximity, which include forming graphene-vdW heterostructures [18, 19] and the adsorption of adatoms like hydrogen [20], fluorine [21] and heavy metals Os [13], Au [22, 23] and In [14]. In all these cases, SOC induced band splitting is in the range of few meV. By their mere proximity the transition metals are capable of imprinting a unique spin texture in graphene electronic bands. So far not much effort has been made in studying the size dependent proximity effect of atomic clusters, presumably because the clusters may aggregate, and their size-selective fabrication and controlled deposition is challenging. Notably, in the work of Scheerder *et al* and Keijers *et al*, size specific adsorption of Au_n clusters ($n = 3$ & 6) on graphene was experimentally demonstrated and the later studied the variation of the induced SOC strength for different cluster sizes [24, 25]. Upon comparing with the spin-splitting obtained from density functional theory (DFT) simulations, they were able to identify the spin

relaxation mechanism of the Au_n clusters/graphene systems as being primarily the Elliot–Yafet (EY) like mechanism.

The additional degree of freedom, provided via the number of atoms in the clusters to tune the electronic properties of graphene, is studied in the present work. More specifically, the size-dependent interaction of Cu_n clusters on pristine and defective (C-vacancy) graphene is investigated, using first-principles simulations based on DFT. Copper is traditionally employed as a substrate for the growth of graphene by chemical vapour deposition [26]. An earlier report suggested that graphene deposited on Cu(111) surface interact through weak van der Waals type bonding [27], which implies copper may induce proximity effects without drastically affecting graphene's properties. Graphene functionalized with copper adatoms was studied by Frank *et al* by employing *ab initio* and tight binding model calculations [28]. Their simulations predicted spin–orbit induced splitting in the order of a few meV, which is three orders of magnitude larger than the intrinsic SOC of pristine graphene of a few μeV [29].

The lowest energy ground state configuration for Cu_n ($n = 1$–5) clusters adsorbed on pristine and defective graphene is first obtained. The induced properties can be altered significantly by the cluster orientation, therefore a site-specific search was made to find the geometrical configuration corresponding to the global minimum. Non-collinear band structure and spin texture calculations are performed to study the induced SOC effects. Apart from inducing spin splitting in the range of few meV, the adsorption of the clusters also strongly modifies the spin texture of the low energy bands of graphene. The breaking of the structural symmetry upon cluster adsorption induces Rashba and spin–valley coupling, resulting in a spin lifetime anisotropy between in-plane and out-of-plane polarized electrons. We show that the size of the adsorbed cluster imparts large variations in the spin texture of graphene monolayers, either with or without defects.

2. Method

DFT simulations, as implemented in the plane wave code Vienna *ab initio* simulation package (VASP), were used to compute the ground state atomic configurations and electronic structures of the graphene/Cu_n ($n = 1$–5) systems [30–33]. The Cu_n clusters were adsorbed on a 5×5 graphene supercell. The z-axis (out-of-plane) of the supercell was set to 20 Å to avoid interlayer interactions with the neighbouring cells. Different adsorption sites were considered for the adsorption of the atomic clusters and the systems were relaxed until the forces between the atoms were less than 25 meV $Å^{-1}$. The spin-polarised DFT calculations were performed using a $11 \times 11 \times 1$ k-point mesh to sample the Brillouin zone [34]. The energy cut-off was set to 520 eV and the width of the Gaussian smearing was set to 0.05 eV. The nonlocal vdW-DF2 exchange-and correlation functionals of Lee *et al* [35–38] were employed in these simulations.

The binding energy of the clusters adsorbed on pristine/defective graphene was estimated using the following relation:

$$BE = E_{g+Cu_n} - E_g - E_{Cu_n},$$

where E_g is the total energy of the pristine/defective graphene without Cu cluster. E_{Cu_n} is the total energy of cluster with n atoms. E_{g+Cu_n} is the total energy of the cluster adsorbed pristine/defective graphene system. The spin texture plots were computed using a 21×21 Γ-centered mesh and the spin expectation values were post-processed using VASPKIT and pyprocar [39, 40].

3. Results and discussion

3.1. Pristine graphene

3.1.1. Structural optimization

The most stable geometries of the isolated copper clusters (with lowest total energies) were first obtained, and the results are in good agreement with the work of Calaminici *et al* for neutral Cu_n clusters [41]. Next, the Cu_n clusters were relaxed on graphene in different initial configurations to find the most stable geometries. The obtained geometries are shown in figure 1(f), and the results are summarized in table 1. These results were obtained for single cluster adsorbed graphene supercell, which would be equivalent to a cluster number density of 7.58×10^{13} cm^{-2}. The clusters are adsorbed with a modest binding energy of −0.3 to −0.8 eV at about 2.2–2.6 Å above the pristine graphene plane, except Cu_5 which is located at a distance of 3.5 Å from the graphene. The adsorption of the cluster induces a slight distortion of the graphene plane, i.e. the bond lengths between the C atoms on which the cluster absorbs and their nearest neighbours is elongated by about 0.01–0.015 Å. The distortion of graphene indicates that the cluster adsorption could

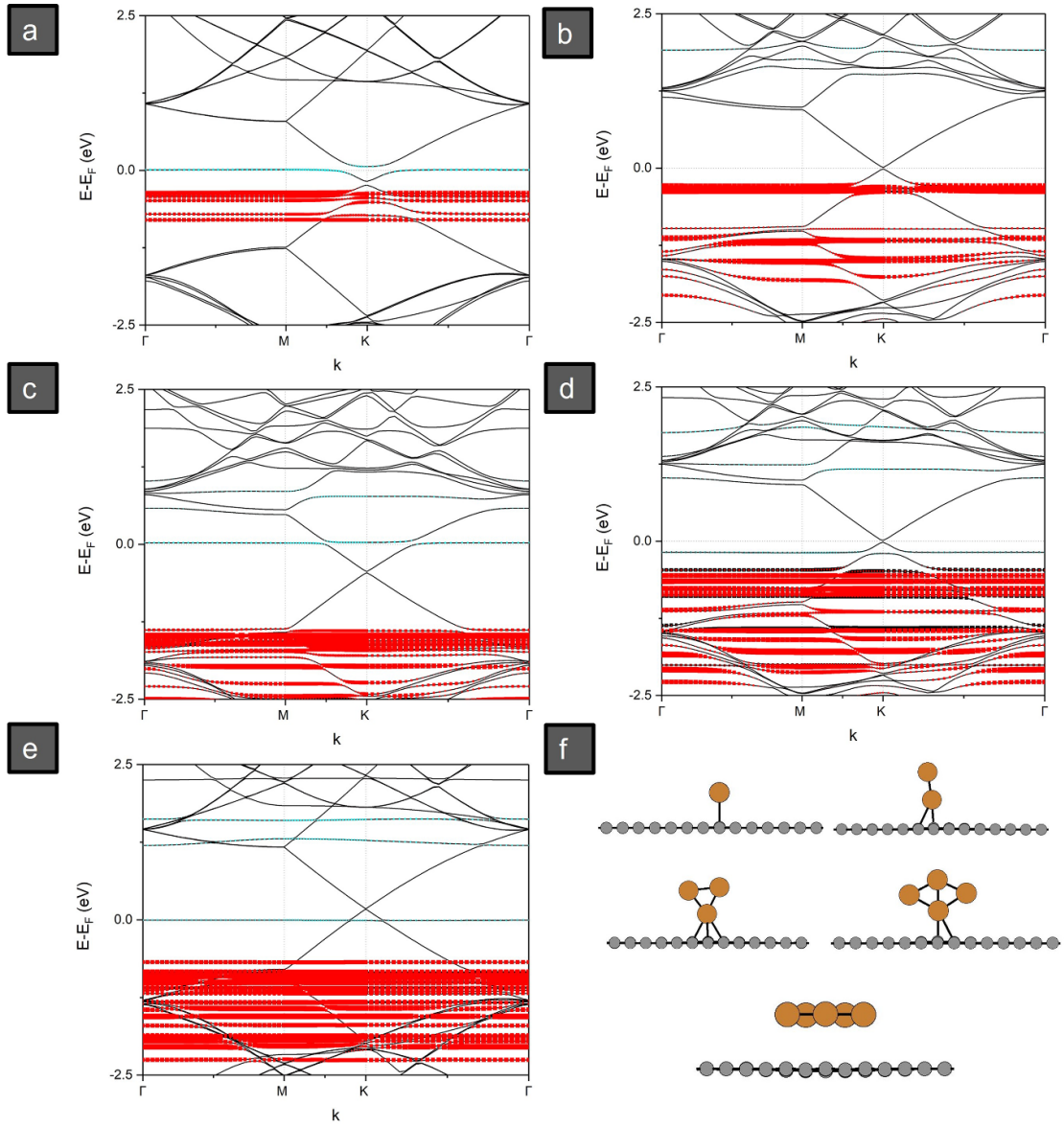

Figure 1. Computed electronic band structures for Cu_n/pristine graphene systems, (a)–(e) for increasing cluster size $n = 1-5$. The projection of Cu s-orbitals and d-orbitals are represented by cyan and red dots, respectively. The size of the dots indicates the magnitude of the projection. (f) The optimised side-view geometry of Cu_n/pristine graphene.

Table 1. Shortest Cu–C bond length, cluster binding energy (BE), and magnetic moment of pristine graphene/Cu_n systems.

Cluster size	Cu–C (Å)	BE (eV)	Magnetic moment (μ_B)
Cu_1	2.64	−0.332	0.91
Cu_2	2.29	−0.486	0
Cu_3	2.18	−0.820	0.79
Cu_4	2.30	−0.688	0
Cu_5	3.53	−0.627	0.97

induce charge transfer and SOC interactions, which will be discussed below. Isolated odd-numbered clusters possess a magnetic moment of ∼1 μ_B due to the presence of an unpaired *s* state. Upon adsorption, the magnetic moment is slightly reduced, due to the interaction of the Cu_n cluster with the graphene plane. For Cu_3/graphene, the cluster moment is reduced to 0.79 μ_B, indicating charge transfer interaction with graphene, and yielding a comparatively larger doping efficiency.

The computed band structures of the Cu_n/graphene systems along the high symmetry points of the Brillouin zone are shown in figures 1(a)–(e). In general, one can observe a hybridization energy gap in the band structure around the Dirac cone (along *M*–*K*–Γ) due to the overlapping copper and carbon orbitals.

Table 2. The obtained values of spin splitting for the Cu_n/pristine graphene system. Only the spin splitting obtained at the Dirac point is provided. Note that the values slightly vary along the K–Γ and M–K paths. CB and VB represent conduction band and valence band, respectively.

Cluster size	Band gap (meV)	CB splitting (meV)	VB splitting (meV)
Cu_1	16.6	28.6	47.2
Cu_2	20.1	1	5
Cu_3	14.32	6	3
Cu_4	25	1.3	2
Cu_5	0.15	1.82	0.62

Especially the Cu d-states (red coloured dots) hybridize with the graphene valence band. In the case of Cu_1/graphene, the flat band observed at the Fermi level corresponds to a mid-gap impurity-like state. A similar band structure was obtained for a Cu adatom on graphene in the work of Frank *et al* [28].

An odd–even oscillation is manifested in the charge transfer process as well. The doping density (n_s) was estimated from the shift of the Dirac cone from the Fermi level (ΔE_F),

$$n_s = \frac{{\Delta E_F}^2}{\pi \hbar^2 v_F^2}$$

where v_F is the Fermi velocity. For Cu_3/graphene, n-type doping is predicted with a doping efficiency of 0.145 e per cluster, and for a Cu_5 cluster on graphene, it results in p-type doping with an efficiency of 0.022 h per cluster. In the case of even-numbered clusters, no doping is observed, but the cluster-induced structural asymmetry between the graphene sublattices results in the opening of an energy gap at the Dirac point, which is 21.9 meV and 26.9 meV for Cu_2/graphene and Cu_4/graphene respectively. These band gaps originate from the breaking of symmetry since the clusters are adsorbed in a top configuration on one of the two sublattices, leading to a symmetric separation of the Dirac cones [20].

The observed oscillation in graphene's doping is also related to the pairing of Cu 4 s electrons. In the case of odd-numbered clusters, the unpaired 4 s states (cyan coloured dots) are close to the Fermi level, resulting in the redistribution of charge, i.e. the 4 s states are involved in the charge transfer. For the even numbered clusters, the paired 4 s states are well below the Fermi level, and predominantly hybridize with the graphene valence band states.

Note that the geometries of the isolated Cu_n clusters are also similar to the Au_n clusters, reported in our previous work [23], since both elements share a similar electronic configuration. However, compared to the Au_n/graphene systems, where the Au_n clusters are weakly chemisorbed (-0.6 to -1.7 eV), the lower binding energies between Cu_n and graphene rather suggest a physisorption process. The physisorption of the clusters results in less distortion of the graphene, with preserved high electron and hole mobilities. Nevertheless, the physiosorbed clusters can induce SOC in graphene, due to the proximity effect and inversion symmetry breaking, which will be discussed in the next section.

3.1.2. SOC and spin texture

The induced SOC effect due to symmetry reduction and proximity effects were studied by performing non-collinear spin-polarized calculations on cluster adsorbed graphene systems. The induced SOC lifts the spin degeneracy, resulting in a band gap opening and spin-splitting of the conduction and valence bands. The obtained results are summarized in table 2 and the energy band structures are provided in the Supplementary Information (figure S2). The observed band gap openings are in the range of ∼15–20 meV (except for $Cu_5 \sim 0.1$ meV). The reduced spin-splitting for Cu_5/graphene could be related to the longer cluster-graphene distance of 3.53 Å. In order to confirm this, we made a single point calculation for a reduced cluster-graphene distance of 2.3 Å (this configuration is 2.38 eV higher in energy than the lowest energy configuration). This resulted in larger spin-splitting of ∼6 meV. Therefore, the spin splitting depends on the cluster size, distance, and adsorption site.

The adsorption of the cluster breaks the inversion symmetry of graphene along the z-axis, leading to a Rashba SOC and momentum-dependent spin splitting [18, 19]. Apart from the Rashba-effect, the broken inversion symmetry also leads to a difference in strength of the pseudospin inversion asymmetry (PIA) SOC for graphene's A and B sublattices. PIA-SOC is manifested by the momentum modulated spin splitting of the bands, i.e. the k-linear spin splitting of bands [19, 42]. When the sublattice symmetry is broken, a different intrinsic SOC arises for the two sublattices, which couples spin and valley, resulting in valley-Zeeman SOC. In contrast to the Rashba-induced splitting, the valley-Zeeman effect leads to the out-of-plane spin

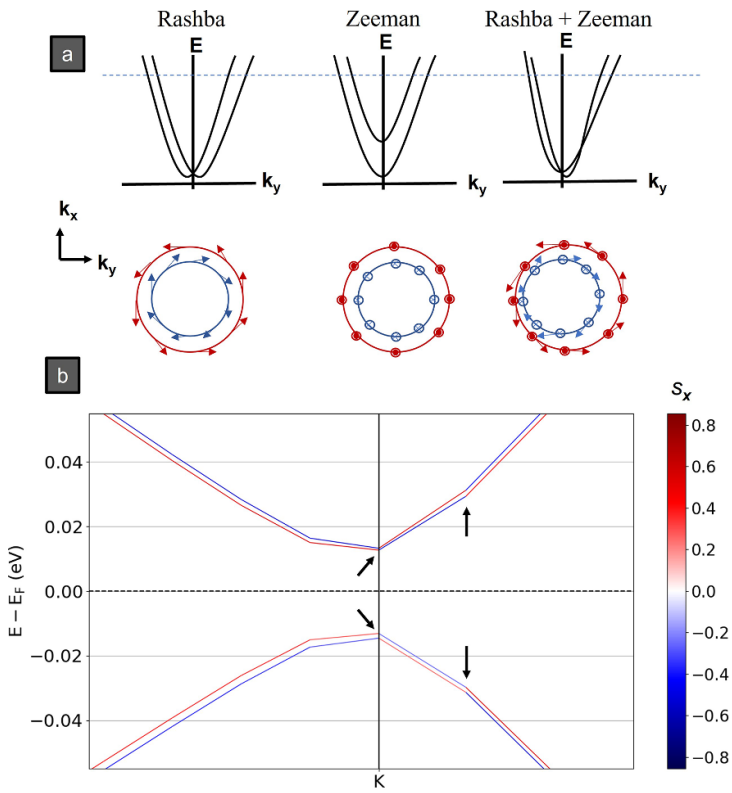

Figure 2. (a) Schematic representation of the effect of Rashba SOC, Zeeman SOC and Rashba + Zeeman SOC, on the band structure (top) and their corresponding Fermi surface along the dotted blue dashed line is shown in the bottom, where the colours represent the spin split bands. In Rashba SOC, the spins are polarised oppositely along the in-plane direction. In Zeeman SOC, the spins are polarised in out-of-plane direction. In Rashba + Zeeman SOC, both in-plane and out-of-plane components are present. (b) Non-collinear band structure of Cu_4/graphene, with band lines projected along the S_x component. The arrows points to crossing between spin up and spin down band, similar to the schematic for Rashba + Zeeman SOC.

polarization, independent of the momentum direction, with opposite signs at the K and K' valleys, to preserve the time reversal symmetry. The interplay of the above-mentioned SOC terms can be observed in the Cu_n/graphene systems and their strengths can be qualitatively highlighted by the spin texture.

In the case of odd-atom clusters with a local magnetic moment, the magnetic anisotropic energy (MAE) of these system can be determined by computing the total energy difference between the out-of-plane (z-axis) and in-plane (x-axis) spin direction ($E(001) - E(100)$). The obtained energies are in the range of 27.5 μeV, -1.52 μeV & -116.5 μeV, respectively, for Cu_1, Cu_3 and Cu_5 adsorbed on graphene. The easy axis orients along the x-axis for Cu_1 and along the z-axis for Cu_3 & Cu_5 clusters. Though MAE ranges within a few μeV, the spins are coupled locally to the magnetic moment of the cluster ($\sim$1 μ_B), leading to the Zeeman-type band splitting, with each subsequent band polarised with spins in opposite directions. Therefore, we observe a momentum independent spin texture (see supplementary information figure S3). This does not imply the absence of Rashba SOC, which still should be present due to the breaking of the inversion symmetry, but the overall spin polarization vector is dominated by the Zeeman SOC.

In the case of even-atom clusters (with no net magnetic moment), due to the coupling of spin and valley, we expect a scenario which is presented in figure 2(a), where the effect of the Rashba and Zeeman contributions on the band structure are schematically drawn. In Rashba (Zeeman) SOC the spin-split bands are polarised oppositely along the in-plane (out-of-plane) direction and their Fermi surface splits into two concentric circle. In the case of combined Rashba and Zeeman SOC, both in-plane and out-of-plane spin components are present, and their resulting spin texture depends on the competition of both terms. For Cu_2 and Cu_4 adsorbed graphene, we expect this particular scenario of Rashba + Zeeman SOC. Figure 2(b) shows the spin-splitted band structure of Cu_4/graphene, where the induced SOC spin splits the band (projected along the S_x component) which shows the presence of both Rashba and Zeeman SOC. In the event of dominant Zeeman SOC, the two concentric circles would be non-equidistantly spaced, as shown by the fermi surface of Rashba + Zeeman SOC (which is observed for Cu_3 on defective graphene, discussed in

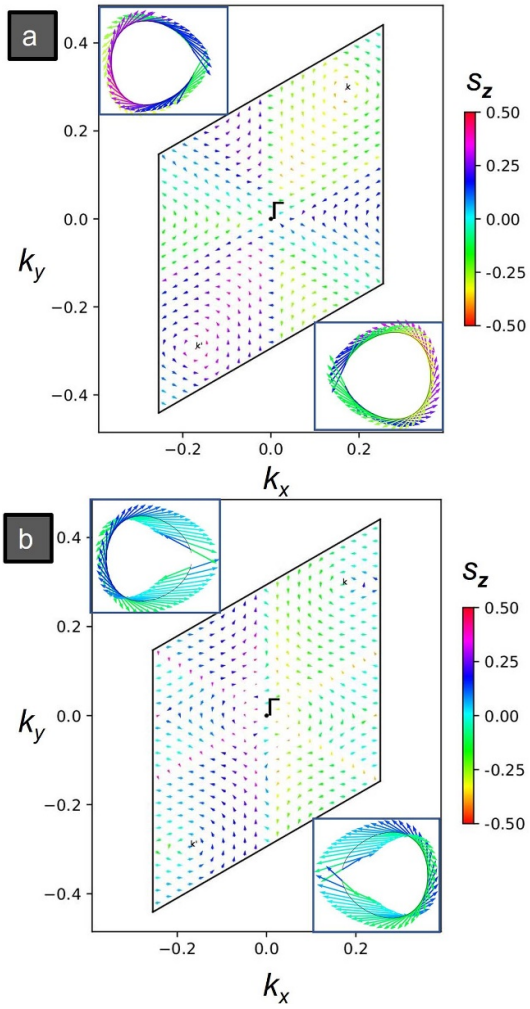

Figure 3. Spin texture plotted for the conduction band minimum of (a) Cu_2/graphene and (b) Cu_4/graphene. The colourbar represents the strength of the $<S_z>$ component, while the in-plane component strength is shown by the length of the arrows. The inset in each plot shows the spin texture along a constant energy surface of ± 0.35 eV from the Fermi level, with top (bottom) inset along the K (K') valley.

section 3.2.2.). The presence of both SOC terms strongly modifies the computed spin expectation values of the graphene bands, as shown in figures 3(a) and (b) for Cu_2/graphene and Cu_4/graphene.

In the case of the Cu_2 cluster-graphene system, the in-plane components of the spin present a chiral spin texture, with a finite out-of-plane S_z component. The in-plane spin components follow the typical Rashba spin texture, due to the breaking of graphene's inversion symmetry. On the other hand, the out-of-plane spin component is driven by the presence of valley-Zeeman and, which arises due to the breaking of sublattice symmetry, and is characterised by the valley dependent polarization of the S_z component. The out-of-plane component of the spin on a constant energy surface is shown in the top and bottom inset of figure 3(a) along the K and K' valley, respectively. The observed 'hedgehog-type' spin texture [43] could be used for potential spintronic applications involving the valley degree of freedom [44, 45].

Interestingly, the in-plane spin component in the Cu_4/graphene system follows a similar chiral texture as in Cu_2/graphene, due to the prevalence of inversion symmetry breaking in both systems. However, the Cu_4/graphene spin texture displays only a very small out-of-plane spin component S_z as evidenced in figure 3(b) and indicated by the (light blue) colourmap near the K and K' valley. This suggests the dominance of the in-plane spin components due to Rashba SOC term over the out-of-plane SOC terms. Consequently, the size of the cluster plays a significant role in favouring certain component of the spins. In comparison with our earlier work on Au_n/graphene systems [23], the induced splitting in Cu_n/graphene is smaller but chiral spin texture was not observed for Au_4/graphene (since the in plane distortion in Au_4/graphene is twice as large as in Cu_4/graphene). This provides the opportunity to engineer Cu_n cluster size dependent spin polarizers, as discussed below.

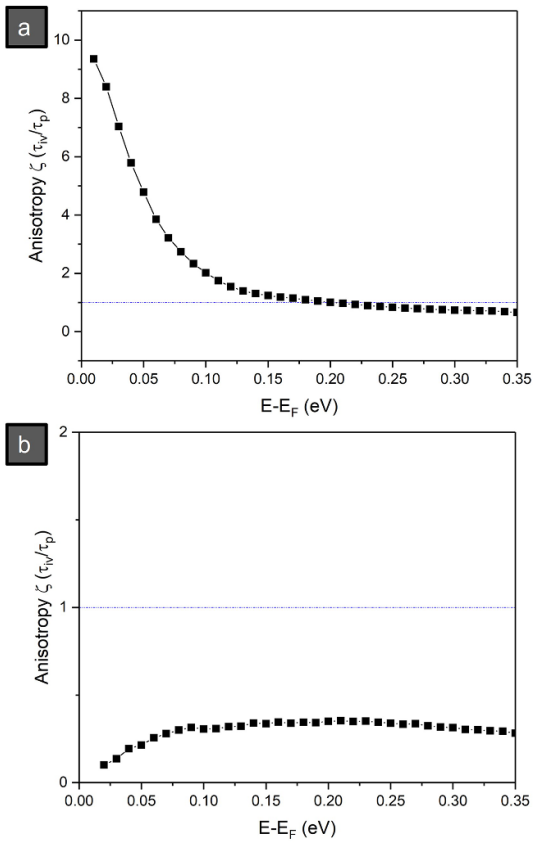

Figure 4. Computed spin lifetime anisotropy as a function of the energy from the Fermi level for (a) Cu_2/graphene and (b) Cu_4/graphene.

3.1.3. Spin lifetime anisotropy

In the literature, the two majorly discussed spin relaxation mechanisms for graphene are the EY and the Dyakonov–Perel (DP) mechanisms [46–48]. In the EY mechanism, each momentum scattering carries a finite probability for spin flip, whereas in the DP mechanism, the electron spin undergoes Larmor's precession in the presence of an SO effective magnetic field [49, 50]. Both mechanisms have different dependences on the momentum lifetime, and their dominance depends on the energy range and carrier density. Assuming that the DP mechanism plays an important role near the Dirac cone, similar to the case of SOC-induced proximity effects between graphene and topological insulators [19], one can extract information about the spin-lifetime anisotropy from the spin texture.

In the DP mechanism, the precession frequency is given by $\omega = \Delta/\hbar$, where Δ is the spin splitting of the bands, and the direction of the effective field $B(k) = \omega S_k$ depends on the momentum direction (due to Rashba SOC). The scattering of electrons influences the spin precession and leads to spin relaxation at a rate given by $\tau_{s,x}^{-1} = \tau_x^* \left(\overline{B(K)}^2 - \overline{B(K)_x^2}\right)$, which randomizes the x-component of the effective magnetic field. In general, it is assumed that $\tau_z^* = \tau_y^* = \tau_x^* = \tau_p$, with τ_p the momentum relaxation time. The spin lifetime anisotropy is defined as the ratio of out-of-plane to in-plane spin relaxation time, which is given by [19]

$$\zeta = \frac{\tau_{s,z}}{\tau_{s,x}} = \frac{\tau_x^* \sum_n \left(\overline{|S^2|} - \overline{S_x^2}\right)_n}{\tau_z^* \sum_n \left(\overline{|S^2|} - \overline{S_z^2}\right)_n},$$

where $S_x^2 = \langle S_x \rangle^2$ is the squared average of the x component of the spin (similarly for the z components). The sum is considered over all four bands near the Fermi surface. Due to the spin–valley coupling in our particular case, there is an additional intervalley scattering time τ_{iv} to the in-plane rate, $\tau_y^{*-1} = \tau_x^{*-1} = \tau_{\mathrm{iv}}^{-1} + \tau_p^{-1}$. Therefore, one gets a spin life-time anisotropy ζ in units of $\frac{\tau_{\mathrm{iv}}}{\tau_p}$.

The computed spin lifetime anisotropy for the conduction band of Cu_2/graphene is shown in figure 4(a) (in the valence band, the flat band due to the contribution of the Cu cluster states comes into play). The anisotropy term becomes larger as one moves closer to the Dirac point, in the range of 10 ($\frac{\tau_{\mathrm{iv}}}{\tau_p}$). Away from the Dirac point, the anisotropy is much reduced, but typically remains larger than 1 till the energy range of

Table 3. The binding energy, bond length, magnetic moment, and spin splitting of Cu_n/defective graphene ($n = 1$–5). Only the spin splitting obtained at the Dirac point is provided. CB and VB represent conduction band and valence band, respectively.

Cluster size	Cu–C (Å)	BE (eV)	Magnetic moment (μ_B)	CB spin splitting (meV)	VB spin splitting (meV)
Cu_1	1.95	−3.62	0.99	150	43.3
Cu_2	1.95–1.99	−2.74	1.92	97	88
Cu_3	1.95–2.04	−3.87	0.57	40	63
Cu_4	1.93–2.12	−3.67	0	7	8
Cu_5	1.98–2.04	−3.93	0.95	65	118

0.2 eV from the Fermi level, indicating longer lifetime for spins polarised in the out-of-plane direction. At higher energy the spin texture is dictated mainly by the Rashba term. Therefore, the average spin lifetime anisotropy collapses below 1. As the anisotropy depends on the ratio of $\frac{\tau_{iv}}{\tau_p}$, and assuming $\tau_{iv} = (5-10)\,\tau_p$ [19], this leads to a substantial difference in spin lifetime for the out-of-plane polarised spins.

Opposed to Cu_2/graphene, the computed anisotropy of Cu_4/graphene is smaller than 1 (figure 4(b)), with the out-of-plane spin relaxation being about three times as fast as the in-plane component. This could be a result of the stronger valley-Zeeman term in Cu_2/graphene with sizable S_z component (colormap in figure 3) in comparison to Cu_4/graphene. Spin lifetime anisotropies have been experimentally observed for graphene/$MoSe_2$ and graphene/WS_2 heterostructures due to the spin proximity effects [51–53]. These results again highlight that the size of the adsorbed cluster is an important 'parameter' that can tune the direction of the spin polarised current in graphene.

3.2. Defective graphene

3.2.1. Geometry

The presence of defects can influence the adsorption of a metal cluster and its induced SOC interaction. We performed simulations on graphene with a single carbon vacancy. Upon introducing a single carbon vacancy in graphene, the Cu_n clusters prefer to adsorb on the defect site, with a higher binding energy in the range of 3 eV (see table 3), indicating chemisorption. The enhanced interaction between the cluster and graphene leads to the deformation of the carbon bonds near the adsorption site, as shown in figures 6(c) and (d). The absence of a single carbon atom in the graphene lattice induces a local magnetic moment ($<2\ \mu_B$). As pointed out in the work of Chen *et al*, the presence of a single vacancy releases four electrons to occupy four localized states, due to a Jahn–Teller distortion [54]. Notably, no net magnetic moment is predicted for the Cu_4 cluster adsorbed on defective graphene. The magnetic moment of the system after the adsorption of the Cu_n cluster is given in supplemental information table 3.

3.2.2. SOC and spin texture

The computed spin polarised electronic band structures of the Cu_n/defective graphene systems are summarized in figure 5. In the case of a single C-vacancy in graphene, the Fermi level lies within the valence band (figure S6), but upon the adsorption of the cluster, the Fermi level shifts closer to the Dirac point (figure 5), indicating charge transfer between the cluster and defective graphene. The MAE of clusters with a local magnetic moment were obtained using the same procedure as mentioned in section 3.1.2 for pristine graphene. In the case of defective graphene, the magnetic moment prefers to orient along the z-axis, with a MAE of −26.2 μeV, −413.6 μeV, −1.17 μeV & −18.5 μeV for Cu_n ($n = 1,2,3\&5$) adsorbed graphene, respectively. The strength of the computed MAE tends to increase with the magnetic moment, which in turn depends on the charge transfer interaction between the cluster and graphene.

The magnitude of the spin-splitting of the conduction and valence bands, as obtained by the non-collinear spin calculations, are provided in table 3. The spin splitting values in defective graphene are much larger than in pristine graphene (table 2) due to the significantly enhanced graphene-cluster interaction. The adsorption of a Cu_n cluster on a C-vacancy also breaks the inversion symmetry along the in-plane direction. This allows for the presence of an out-of-plane component in the spin polarization vectors. The computed band structures and the corresponding spin textures are shown in figure 6 for Cu_3 and Cu_4 clusters adsorbed on defective graphene.

In the case of Cu_3, we observe a complete out-of-plane polarization, with negligible in-plane spin component. The observed spin texture indicates a dominant Zeeman SOC term, originating from the lack of in-plane inversion symmetry and the presence of a local magnetic moment [55]. A small Rashba SOC is also present, due to the symmetry reduction in the out-of-plane direction. From the Fermi contour in figures 6 (a) and (d), an uneven shift of the spin-split bands can be observed (along the k_y direction), confirming the

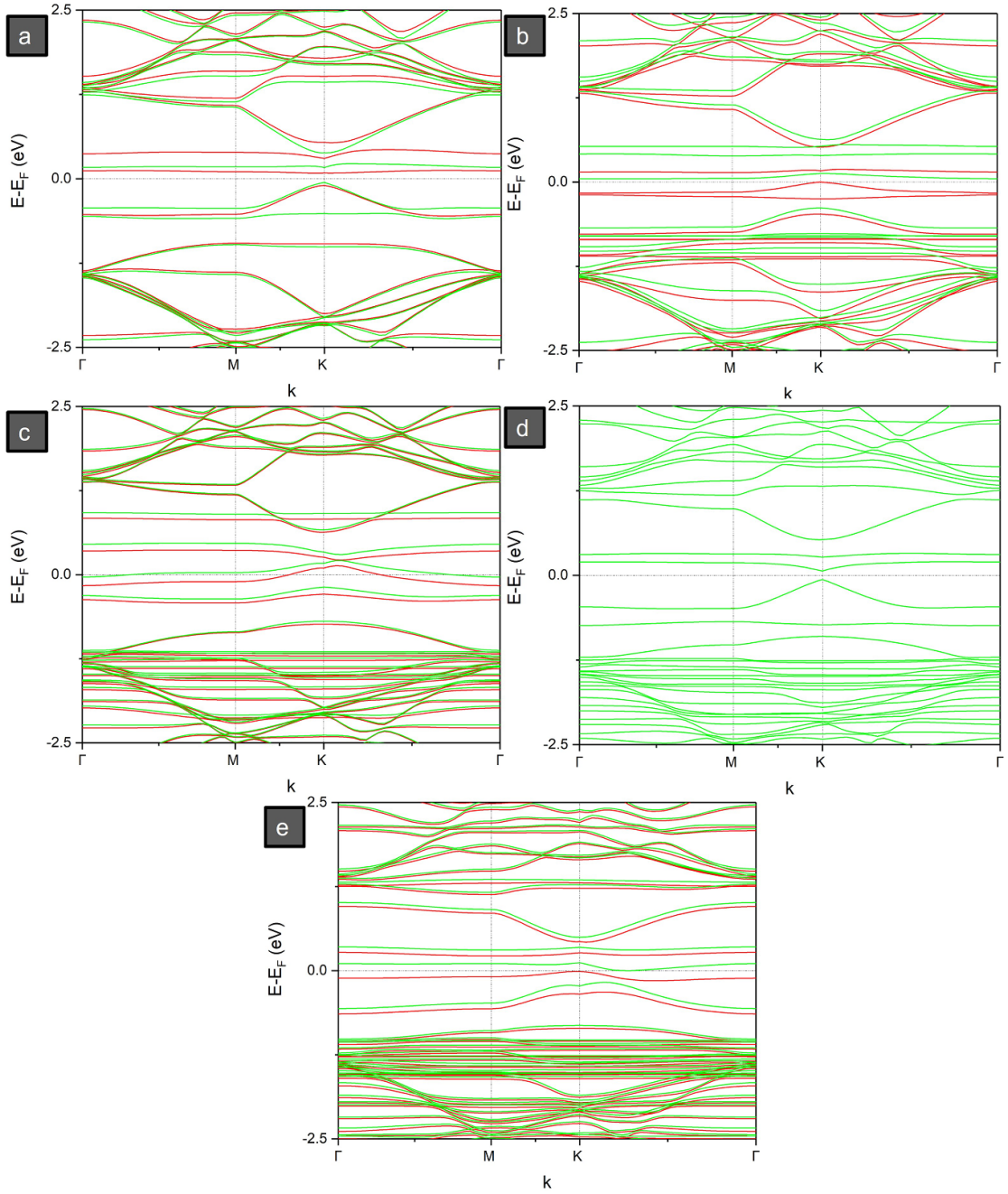

Figure 5. Spin polarised band structure of Cu_n/defective (single C vacancy) graphene, (a)–(e) for increasing cluster size from $n = 1$ to $n = 5$.

manifestation of a combination of Rashba and Zeeman SOC (figure 2(a)). Similar spin textures were observed for Cu_n ($n = 1,2,5$) adsorbed systems, i.e. the polarisation of the split bands is in opposite direction, and they align precisely in the out-of-plane direction. These results are provided in the supplementary information (see figure S5).

On the other hand, the net magnetic moment of the Cu_4/defective-graphene system is zero. In this case, the Rashba SOC term becomes dominant (like in the Cu_4/pristine graphene system) and allows for the presence of the in-plane component of the spin polarization vectors. The cumulative effect of in-plane and out-of-plane inversion symmetry breaking also enhances the band splitting, as compared to the Cu_4/pristine graphene system (2 meV). In addition, since the in-plane spin components are momentum dependent, and the out-of-plane components are coupled with the valley, the spin life-time anisotropy ζ can be computed, as mentioned in section 3.1.3. Note that the results are presented here for the valence band, due to the prevalence of Cu states at the conduction band edge. The obtained results are plotted in figure 7. The

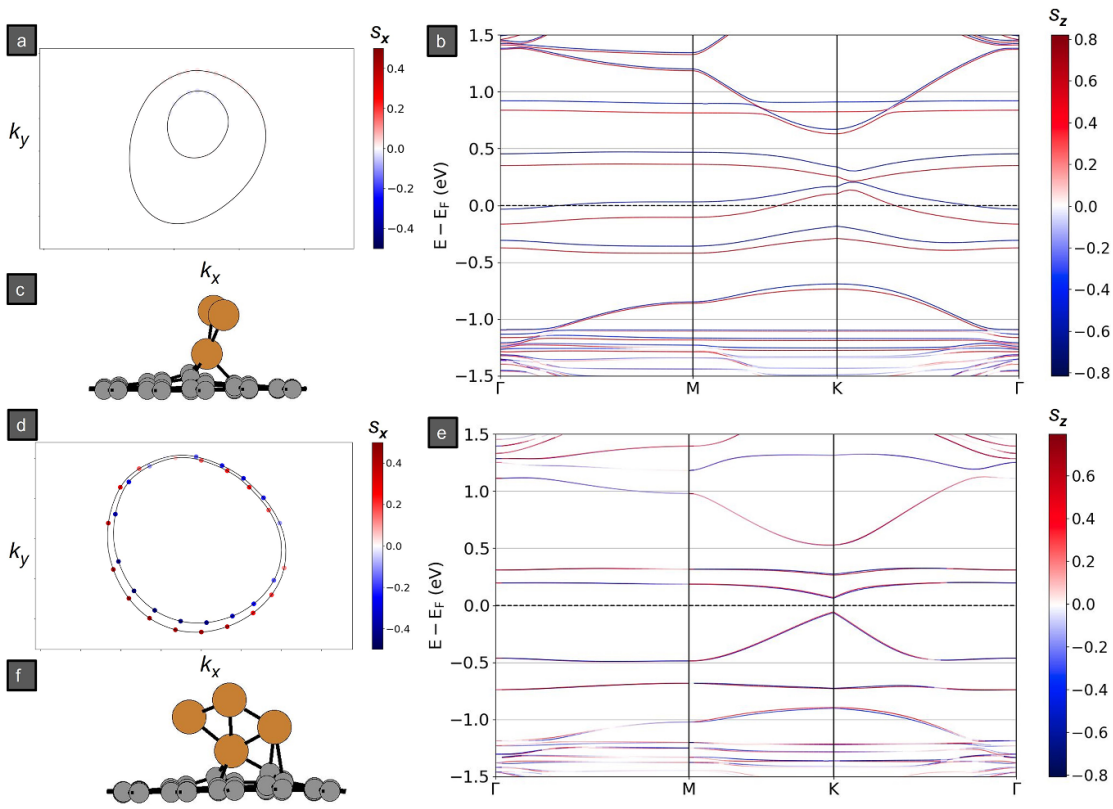

Figure 6. (a) and (d) S_x spin component projected constant energy surface for Cu_3/defective-graphene and Cu_4/defective-graphene, respectively. As can be seen in fermi surface (a) for cluster with magnetic moment there is no in-plane component and in (a) and (d) the fermi surface of spin split Dirac cones are non-equidistantly spaced (similar to schematic of figure 2(a) for Rashba + Zeeman SOC). (b) and (e) S_z spin component projected band structure for Cu_3/defective-graphene and Cu_4/defective-graphene, respectively. (c) and (f) the lowest energy geometrical configuration for Cu_3/defective-graphene and Cu_4/defective-graphene, respectively.

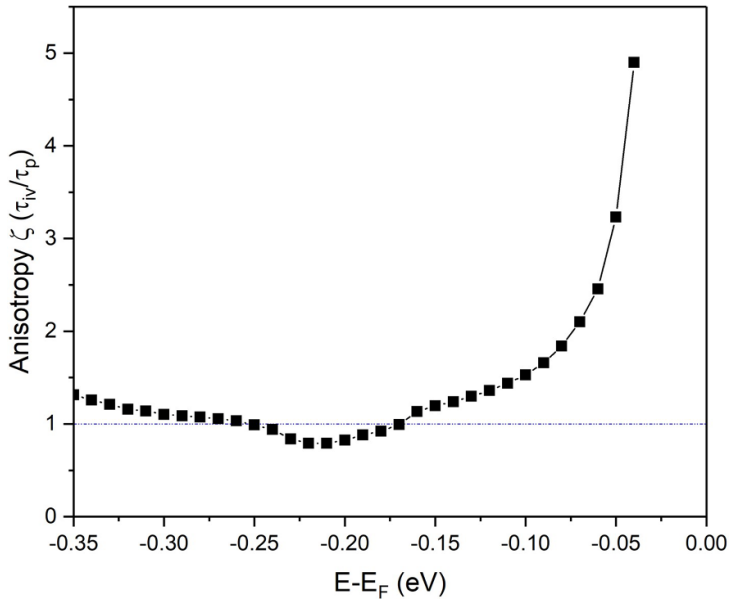

Figure 7. The computed spin lifetime anisotropy for Cu_4/defective graphene.

anisotropy is largest closer to the band edge and decreases at higher energies, reaching a value which is higher than 1, thereby favouring out-of-plane spin polarisation. It could be seen that at energies between −0.17 eV to −0.25 eV the anisotropy drops to ∼0.8 ($\frac{\tau_{iv}}{\tau_p}$). The underlying reason for these minima is unclear. Note,

however, that intervalley scattering is caused by structural defects like vacancies, therefore it could be in the same range as the momentum scattering, leading to an isotropic spin relaxation.

4. Conclusions

First-principles calculations, based on DFT, were performed to study the interaction of few atom Cu_n clusters with pristine and defective (C-vacancy) graphene. The simulations indicate that Cu_n clusters are physiosorbed on pristine graphene with binding energies in the range of ∼0.5 eV. The presence of a C-vacancy on the graphene supercell leads to a much stronger interaction with the Cu clusters, as well as the deformation of the graphene monolayer near the vacancy site.

Non-collinear calculations were performed to study the induced SOC by the proximity of the Cu_n clusters. The induced SOC strength shows a variation with the size of the adsorbed cluster, with different spin splitting values for the low energy bands. The computed spin texture depends on the local magnetic moment induced by the cluster. For clusters on pristine graphene without net magnetic moment, like Cu_2 and Cu_4, a Rashba-type chiral spin texture is observed with a significant spin–valley coupling. Similarly, in the case of a Cu_4 cluster adsorbed on a single vacancy graphene site (with net zero magnetic moment), the spin–valley coupling is also predicted and is found to arise from the interplay between the Rashba and in-plane Zeeman terms. For other clusters adsorbed on defective graphene, a complete out-of-plane spin texture is predicted, due to breaking of the in-plane inversion symmetry.

The breaking of the sub-lattice symmetry and $z/-z$ inversion symmetry could induce a spin lifetime anisotropy, within the Dyakonov–Perel regime. From our simulations, we expect a larger spin lifetime for the out-of-plane spin component for the Cu_2/graphene system. In the case of Cu_4/graphene, the scenario is inversed with the out-of-plane spin component being relaxed twice as fast as the in-plane component. The difference in behaviour is due to different dominating SOC terms in each system, which in turn depends on the size and orientation of the adsorbed cluster. This offers a possibility to design spin polarizers by precisely depositing size-selected clusters on graphene. The presence of defects and disorder can significantly impact the spin texture and spin lifetime, e.g. a Cu_4 cluster on defective graphene showed a different trend in comparison to the pristine graphene counterpart. These findings highlight that the size of the deposited Cu clusters can have a significant impact on graphene's electronic and spin properties. Therefore, proper engineering along with *ab initio* calculations could guide towards maximizing the use of atomic clusters as a tool to functionalize graphene-based devices.

Data availability statement

The data cannot be made publicly available upon publication because no suitable repository exists for hosting data in this field of study. The data that support the findings of this study are available upon reasonable request from the authors.

Acknowledgments

This work has been financially supported by the Research Foundation-Flanders (FWO Project G.0D56.19N) and by the KU Leuven Internal Research Funds C14/21/083. Part of the computational resources and services used in this work have been provided by the VSC (Flemish Supercomputer Center), funded by the Research Foundation-Flanders (FWO) and the Flemish Government-department EWI.

ORCID iDs

Ramasamy Murugesan https://orcid.org/0000-0001-6294-7206
Ewald Janssens https://orcid.org/0000-0002-5945-1194
Joris Van de Vondel https://orcid.org/0000-0001-6894-7258
Valeri Afanas'ev https://orcid.org/0000-0001-5018-4539

References

[1] Novoselov K S, Geim A K, Morozov S V, Jiang D E, Zhang Y, Dubonos S V, Grigorieva I V and Firsov A A 2004 Electric field effect in atomically thin carbon films *Science* **306** 666–9
[2] Schaibley J R, Yu H, Clark G, Rivera P, Ross J S, Seyler K L, Yao W and Xu X 2016 Valleytronics in 2D materials *Nat. Rev. Mater.* **1** 16055
[3] Glavin N R, Rao R, Varshney V, Bianco E, Apte A, Roy A, Ringe E and Ajayan P M 2020 Emerging applications of elemental 2D materials *Adv. Mater.* **32** 1904302
[4] Gupta A, Sakthivel T and Seal S 2015 Recent development in 2D materials beyond graphene *Prog. Mater. Sci.* **73** 44–126

[5] Kurebayashi H, Garcia J H, Khan S, Sinova J and Roche S 2022 Magnetism, symmetry and spin transport in van der Waals layered systems *Nat. Rev. Phys.* **4** 150–66
[6] Leutenantsmeyer J C, Kaverzin A A, Wojtaszek M and van Wees B J 2016 Proximity induced room temperature ferromagnetism in graphene probed with spin currents *2D Mater.* **4** 14001
[7] Wang Z, Tang C, Sachs R, Barlas Y and Shi J 2015 Proximity-induced ferromagnetism in graphene revealed by the anomalous Hall effect *Phys. Rev. Lett.* **114** 16603
[8] Trainer D J, Wang B, Bobba F, Samuelson N, Xi X, Zasadzinski J, Nieminen J, Bansil A and Iavarone M 2020 Proximity-induced superconductivity in monolayer MoS_2 *ACS Nano* **14** 2718–28
[9] Efetov D K *et al* 2016 Specular interband Andreev reflections at van der Waals interfaces between graphene and $NbSe_2$ *Nat. Phys.* **12** 328–32
[10] Bretheau L, Wang -J I-J, Pisoni R, Watanabe K, Taniguchi T and Jarillo-Herrero P 2017 Tunnelling spectroscopy of Andreev states in graphene *Nat. Phys.* **13** 756–60
[11] Popov I, Mantega M, Narayan A and Sanvito S 2014 Proximity-induced topological state in graphene *Phys. Rev.* B **90** 35418
[12] Huang H, Xu Y, Wang J and Duan W 2017 Emerging topological states in quasi-two-dimensional materials *WIREs Comput. Mol. Sci.* **7** e1296
[13] Hu J, Alicea J, Wu R and Franz M 2012 Giant topological insulator gap in graphene with *5d* adatoms *Phys. Rev. Lett.* **109** 266801
[14] Weeks C, Hu J, Alicea J, Franz M and Wu R 2011 Engineering a robust quantum spin Hall state in graphene via adatom deposition *Phys. Rev.* X **1** 021001
[15] Takiguchi K, Anh L D, Chiba T, Koyama T, Chiba D and Tanaka M 2019 Giant gate-controlled proximity magnetoresistance in semiconductor-based ferromagnetic–non-magnetic bilayers *Nat. Phys.* **15** 1134–9
[16] Sajadi E, Palomaki T, Fei Z, Zhao W, Bement P, Olsen C, Luescher S, Xu X, Folk J A and Cobden D H 2018 Gate-induced superconductivity in a monolayer topological insulator *Science* **362** 922–5
[17] Costanzo D, Jo S, Berger H and Morpurgo A F 2016 Gate-induced superconductivity in atomically thin MoS_2 crystals *Nat. Nanotechnol.* **11** 339–44
[18] Gmitra M, Kochan D, Högl P and Fabian J 2016 Trivial and inverted Dirac bands and the emergence of quantum spin Hall states in graphene on transition-metal dichalcogenides *Phys. Rev.* B **93** 155104
[19] Song K, Soriano D, Cummings A W, Robles R, Ordejón P and Roche S 2018 Spin proximity effects in graphene/topological insulator heterostructures *Nano Lett.* **18** 2033–9
[20] Gmitra M, Kochan D and Fabian J 2013 Spin-orbit coupling in hydrogenated graphene *Phys. Rev. Lett.* **110** 246602
[21] Irmer S, Frank T, Putz S, Gmitra M, Kochan D and Fabian J 2015 Spin-orbit coupling in fluorinated graphene *Phys. Rev.* B **91** 115141
[22] Ma D, Li Z and Yang Z 2012 Strong spin–orbit splitting in graphene with adsorbed Au atoms *Carbon* **50** 297–305
[23] Murugesan R, Meng R, de Volder A, Keijers W, Janssens E, Van de Vondel J, Afanasiev V and Houssa M 2022 Interaction of graphene with Au_n clusters: a first-principles study *J. Phys.: Condens. Matter* **34** 405701
[24] Scheerder J E, Liu S, Zharinov V S and Reckinger N 2018 Electronic detection of oxygen adsorption and size-specific doping of few-atom gold clusters on graphene *Adv. Mater. Interfaces* **5** 1801274
[25] Keijers W, Murugesan R, Libeert G, Scheerder J E, Raes B, Brems S, De Gendt S, Houssa M, Janssens E and Van de Vondel J 2021 Tuning the spintronic properties of graphene with atomically precise Au clusters *J. Phys. Mater.* **4** 45005
[26] Mattevi C, Kim H and Chhowalla M 2011 A review of chemical vapour deposition of graphene on copper *J. Mater. Chem.* **21** 3324–34
[27] Frank T, Gmitra M and Fabian J 2016 Theory of electronic and spin-orbit proximity effects in graphene on Cu(111) *Phys. Rev.* B **93** 155142
[28] Frank T, Irmer S, Gmitra M, Kochan D and Fabian J 2017 Copper adatoms on graphene: theory of orbital and spin-orbital effects *Phys. Rev.* B **95** 35402
[29] Konschuh S, Gmitra M and Fabian J 2010 Tight-binding theory of the spin-orbit coupling in graphene *Phys. Rev.* B **82** 245412
[30] Kresse G and Hafner J 1993 *Ab initio* molecular dynamics for liquid metals *Phys. Rev.* B **47** 558–61
[31] Kresse G and Furthmüller J 1996 Efficiency of *ab-initio* total energy calculations for metals and semiconductors using a plane-wave basis set *Comput. Mater. Sci.* **6** 15–50
[32] Kresse G and Joubert D 1999 From ultrasoft pseudopotentials to the projector augmented-wave method *Phys. Rev.* B **59** 1758–75
[33] Blöchl P E 1994 Projector augmented-wave method *Phys. Rev.* B **50** 17953–79
[34] Monkhorst H J and Pack J D 1976 Special points for Brillouin-zone integrations *Phys. Rev.* B **13** 5188–92
[35] Klimeš J, Bowler D R and Michaelides A 2009 Chemical accuracy for the van der Waals density functional *J. Phys.: Condens. Matter* **22** 22201
[36] Klimeš J, Bowler D R and Michaelides A 2011 Van der Waals density functionals applied to solids *Phys. Rev.* B **83** 195131
[37] Dion M, Rydberg H, Schröder E, Langreth D C and Lundqvist B I 2004 Van der Waals density functional for general geometries *Phys. Rev. Lett.* **92** 246401
[38] Lee K, Murray É D, Kong L, Lundqvist B I and Langreth D C 2010 Higher-accuracy van der Waals density functional *Phys. Rev.* B **82** 81101
[39] Wang V, Xu N, Liu J-C, Tang G and Geng W-T 2021 VASPKIT: a user-friendly interface facilitating high-throughput computing and analysis using VASP code *Comput. Phys. Commun.* **267** 108033
[40] Herath U, Tavadze P, He X, Bousquet E, Singh S, Muñoz F and Romero A H 2020 PyProcar: a Python library for electronic structure pre/post-processing *Comput. Phys. Commun.* **251** 107080
[41] Calaminici P, Köster A M, Russo N and Salahub D R 1996 A density functional study of small copper clusters: Cu_n ($n \leqslant 5$) *J. Chem. Phys.* **105** 9546–56
[42] Pezo A, Zanolli Z, Wittemeier N, Ordejón P, Fazzio A, Roche S and Garcia J H 2021 Manipulation of spin transport in graphene/transition metal dichalcogenide heterobilayers upon twisting *2D Mater.* **9** 15008
[43] Varykhalov A, Sánchez-Barriga J, Marchenko D, Hlawenka P, Mandal P S and Rader O 2015 Tunable Fermi level and hedgehog spin texture in gapped graphene *Nat. Commun.* **6** 7610
[44] Xiao D, Yao W and Niu Q 2007 Valley-contrasting physics in graphene: magnetic moment and topological transport *Phys. Rev. Lett.* **99** 236809
[45] Tsai W-F, Huang C-Y, Chang T-R, Lin H, Jeng H-T and Bansil A 2013 Gated silicene as a tunable source of nearly 100% spin-polarized electrons *Nat. Commun.* **4** 1500

[46] Dyakonov M I and Perel V I 1972 Spin relaxation of conduction electrons in noncentrosymmetric semiconductors *Sov. Phys. Solid State* **13** 3023–6
[47] Elliott R J 1954 Theory of the effect of spin-orbit coupling on magnetic resonance in some semiconductors *Phys. Rev.* **96** 266–79
[48] Yafet Y 1952 Calculation of the *g* factor of metallic sodium *Phys. Rev.* **85** 478
[49] Fabian J, Matos-Abiague A, Ertler C, Stano P and Zutic I 2007 Semiconductor spintronics *Acta Phys. Slovaca* **57** 565–907
[50] Cummings A W, Garcia J H, Fabian J and Roche S 2017 Giant spin lifetime anisotropy in graphene induced by proximity effects *Phys. Rev. Lett.* **119** 206601
[51] Benítez L A, Sierra J F, Savero Torres W, Arrighi A, Bonell F, Costache M V and Valenzuela S O 2018 Strongly anisotropic spin relaxation in graphene–transition metal dichalcogenide heterostructures at room temperature *Nat. Phys.* **14** 303–8
[52] Ghiasi T S, Ingla-Aynés J, Kaverzin A A and van Wees B J 2017 large proximity-induced spin lifetime anisotropy in transition-metal dichalcogenide/graphene heterostructures *Nano Lett.* **17** 7528–32
[53] Zihlmann S, Cummings A W, Garcia J H, Kedves M, Watanabe K, Taniguchi T, Schönenberger C and Makk P 2018 Large spin relaxation anisotropy and valley-Zeeman spin-orbit coupling in WSe_2/graphene/*h*-BN heterostructures *Phys. Rev.* B **97** 75434
[54] Chen J-J, Wu H-C, Yu D-P and Liao Z-M 2014 Magnetic moments in graphene with vacancies *Nanoscale* **6** 8814–21
[55] Uchihashi T 2021 Surface atomic-layer superconductors with Rashba/Zeeman-type spin-orbit coupling *AAPPS Bull.* **31** 27